ADVANCED FUNCTIONAL MATERIALS
www.afm-journal.de

Constructing Conductive Interfaces between Nickel Oxide Nanocrystals and Polymer Carbon Nitride for Efficient Electrocatalytic Oxygen Evolution Reaction

Chengan Liao, Baopeng Yang, Ning Zhang, Min Liu, Guoxin Chen, Xiaoming Jiang, Gen Chen, Junliang Yang, Xiaohe Liu,* Ting-Shan Chan, Ying-Jui Lu, Renzhi Ma,* and Wei Zhou*

Combining transition metal oxide catalysts with conductive carbonaceous material is a feasible way to improve the conductivity. However, the electrocatalytic performance is usually not distinctly improved because the interfacial resistance between metal oxides and carbon is still large and thereby hinders the charge transport in catalysis. Herein, the conductive interface between poorly conductive NiO nanoparticles and semi-conductive carbon nitride (CN) is constructed. The NiO/CN exhibits much-enhanced oxygen evolution reaction (OER) performance than corresponding NiO and CN in electrolytes of KOH solution and phosphate buffer saline, which is also remarkably superior over NiO/C, commercial RuO_2, and mostly reported NiO-based catalysts. X-ray photoelectron spectroscopy and extended X-ray absorption fine structure spectrum reveal that a metallic Ni–N bond is formed between NiO and CN. Density functional theory calculations suggest that NiO and CN linked by a Ni–N bond possess a low Gibbs energy for OER intermediate adsorptions, which not only improves the transfer of charge but also promotes the transmission of mass in OER. The metal–nitrogen bonded conductive and highly active interface pervasively exists between CN and other transition metal oxides including Co_3O_4, CuO, and Fe_2O_3, making it promising as an inexpensive catalyst for efficient water splitting.

1. Introduction

The overall water splitting is usually high energy demand due to the sluggish kinetics in oxygen evolution reaction (OER).[1–3] Although most scarce and high cost catalysts such as RuO_2 and IrO_2 are applied, the efficiency are still frustratingly low.[4] Developing efficient and cost-effective OER electrocatalysts is of great importance.[5] To date, numerable catalysts composed of transition-metal oxides,[6–10] hydroxides,[11–14] phosphides,[15,16] and sulfides[17,18] have been developed as low-cost alternatives to precious metal compounds. Among them, the transition-metal oxides including NiO, Co_2O_3, Fe_2O_3, etc. are widely devoted as superior catalysts for OER arisen from their stable chemical property and facile preparation procedure.[4,7,19,20] However, most metal oxides have the poor conductivity, which hinders the transport of charge carries and results in low OER efficiency. To improve conductivity of whole electrodes

C. Liao, B. Yang, Prof. N. Zhang, Prof. G. Chen, Prof. X. Liu
School of Materials Science and Engineering
Central South University
Changsha, Hunan 410083, P. R. China
E-mail: nzhang@csu.edu.cn; liuxh@csu.edu.cn
Prof. M. Liu, Prof. J. Yang
School of Physical Science and Electronics
Central South University
Changsha, Hunan 410083, P. R. China
Prof. X. Jiang
State Key Lab of Structural Chemistry
Fujian Institute of Research on the Structure of Matter
Chinese Academy of Sciences
Fuzhou, Fujian 350002, P. R. China
Prof. G. Chen
Ningbo Institute of Materials Technology & Engineering
Chinese Academy of Sciences
No. 1219 Zhongguan West Road Zhenhai District
Ningbo, Zhejiang 315201, P. R. China
T.-S. Chan, Y.-J. Lu
National Synchrotron Radiation Research Center, Taiwan
101 Hsin Ann Road, Hsinchu Science Park
Hsinchu 30076, Taiwan, P. R. China
Prof. R. Ma, Prof. W. Zhou
International Center for Materials Nanoarchitectonics (MANA)
National Institute for Materials Science (NIMS)
1-1 Namiki, Tsukuba, Ibaraki 305-0044, Japan
E-mail: ma.renzhi@nism.go.jp

The ORCID identification number(s) for the author(s) of this article can be found under https://doi.org/10.1002/adfm.201904020.

DOI: 10.1002/adfm.201904020

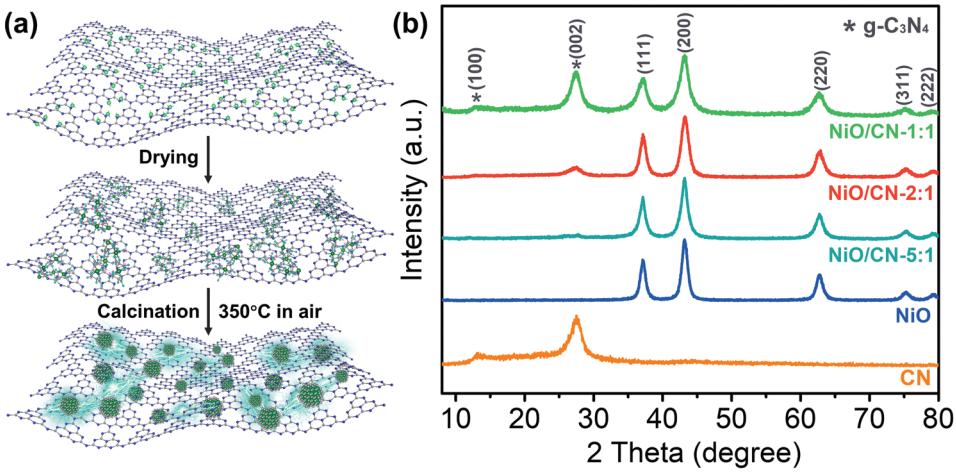

Figure 1. a) Schematic diagram of synthetic process for NiO/CN; b) XRD patterns of as synthesized NiO/CN-1:1, NiO/CN-2:1, NiO/CN-5:1, NiO, and CN.

and facilitate the transfer of charge carries, most transition metal-based compounds were composited with conductive substrates such as MoS_2,[17,21] black phosphorus,[22,23] and conductive carbonaceous material.[24–27] However, the electrochemical performance is usually not improved distinctly via such a composition strategy due to that the interfacial resistances between substrate and active materials are still large. Such a problem would hinder the charge transfer and induce the poor performance of OER. In this regard, constructing conductive interfaces to accelerate the transfer of charge carries is important.

As a famous semiconductive polymer, polymer carbon nitride (generally known as g-C_3N_4) attracts extensive attention for its intriguing properties such as environmental-friendly, low-cost, elements earth-abundant, and facile synthesis.[28–30] Because of the chemical and mechanical stability as well as strong tolerance to acid and alkaline environments, carbon nitride materials (CN) are recently used as substrates for dispersing high conductive metal nanoparticles (e. g. Pd, Pt, and Cu) and graphene to reduce the particles aggregation during catalysis.[31,32] However, CN composited with transition metal oxides for OER is seldom concerned. That is because carbon nitride is usually electrochemical inactive and poor conductivity; high conductivity of whole catalyst will not be produced if this material simply contacts with some poor conductive transition metal oxides. Recently, a few studies have shown that the surficial structure and interfacial interactions have a significant effect on the performance of catalytic behavior,[7,32] which means that the catalytic activity can be enhanced by tuning the surficial and interfacial atom environment. In this regard, constructing highly conductive interfaces by properly interacting transition metal oxides with CN will probably promote charge transport and subsequently the OER performance.

In this study, a facile in situ decomposition method is developed to synthesizing nickel oxides nanocrystals on carbon nitride (NiO/CN) with high conductive interfaces. The NiO nanocrystals anchored CN show distinctly reduced OER overpotential and enhanced stability than corresponding single phased NiO and CN in alkaline KOH solution and neutral phosphatic buffer saline (PBS). The OER activity also is much superior to the carbon supported NiO (NiO/C), commercial RuO_2, and most reported NiO-based catalysts. X-ray photoelectron spectroscopy and extended X-ray absorption fine structure spectra reveal that metallic Ni–N bond are generated between NiO and polymer carbon nitride. Calculations by density functional theory (DFT) have explained that NiO/CN interface with the existence of Ni–N bond has a low adsorption Gibbs energy of OER, which associate with low adsorptive resistance of intermediates and is favorable to the OER process. Such conductive interface exists not only between NiO and CN, but also exists in interfaces between CN and other transition metal oxides including Co_2O_3, CuO, Fe_2O_3, and so on. In addition, the application of as prepared NiO/CN is demonstrated in a device of photovoltaic water electrolysis from crystalline silicon solar cell, which produces a high energy conversion efficiency of 5.35% from solar to hydrogen. This work suggests that highly efficient OER catalysts can be designed through constructing conductive interfaces between transition metal oxides and polymer carbon nitride, which is promising as low-cost catalysts for water splitting.

2. Results and Discussion

The growth of NiO nanocrystals on CN nanosheets is illustrated in **Figure 1**a. First, the Ni^{2+} from the dissolved $Ni(CH_3COO)_2 \cdot 4H_2O$ is adsorbed in surface of CN (e. g. the g-C_3N_4). After drying, the Ni^{2+} salt particle (almost $Ni(CH_3COO)_2 \cdot 4H_2O$) is attached on the surface of CN. Finally, the NiO nanocrystals are produced through the decomposition of Ni^{2+} salt in air via the high-temperature calcination. The composition and crystal structure of all products were characterized the powder X-ray diffraction (XRD). As displayed in Figure 1b, the diffraction peaks for bare product of nickel oxide are consistent with cubic phase NiO (JCPDS card No. 47-1049). The diffraction pattern for polymer carbon nitride is close to the widely reported g-C_3N_4, which has a layered graphitic structure.[33,34] For the composited products, the intensity of CN becomes weaker and intensity of NiO increases with improved content of NiO from NiO/CN-1:1 to NiO/CN-5:1. In addition, there is no other impurity observed from the X-ray

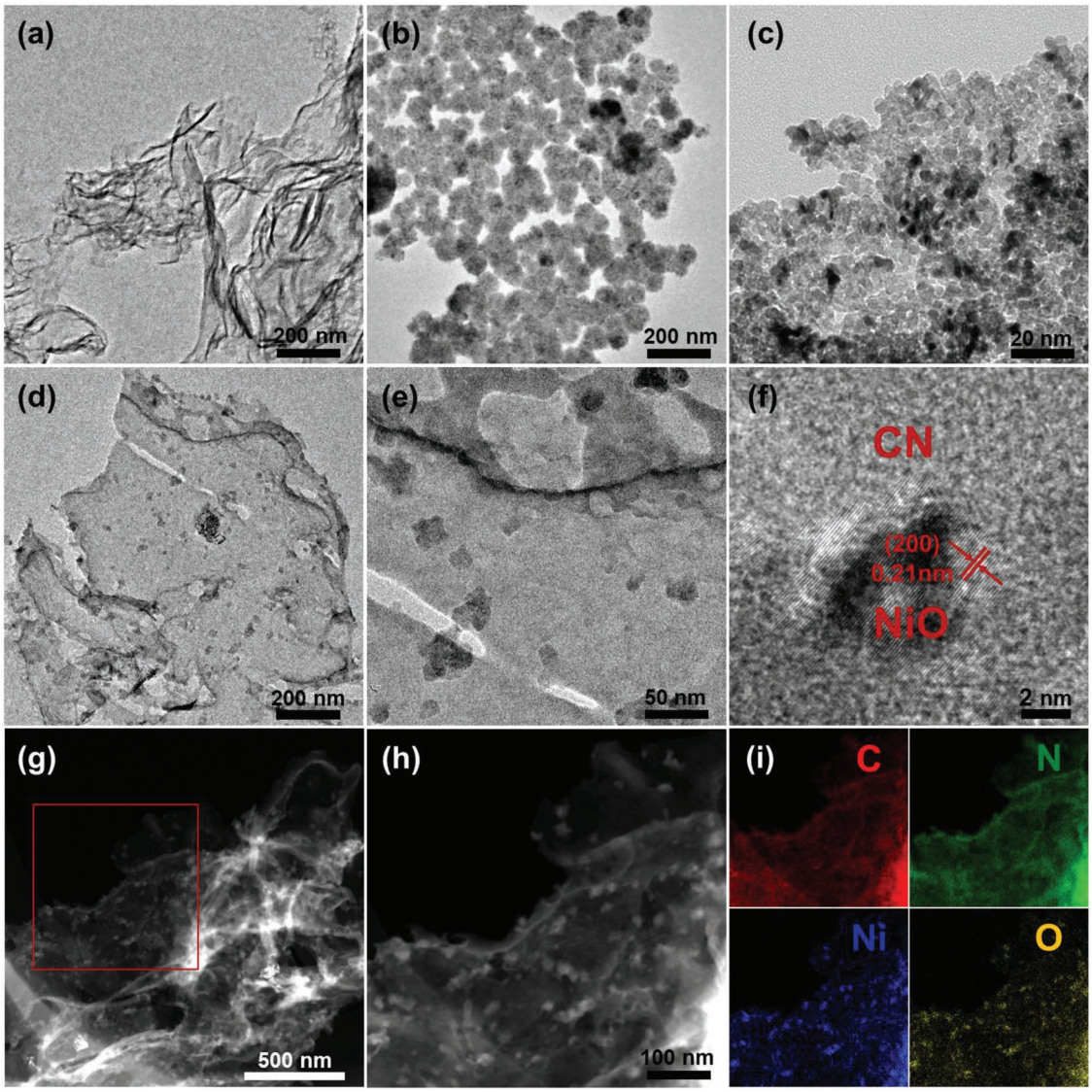

Figure 2. The TEM images of a) CN, b,c) NiO, and d,e) NiO/CN-2:1; f) the HRTEM image of NiO/CN-2:1; g,h) HAADF-STEM images of NiO/CN-2:1 and i) corresponding elemental EDX mappings.

diffraction (XRD) patterns, indicating that the product contains only double components of NiO and CN. The ratio of NiO and CN for NiO/CN-1:1, NiO/CN-2:1, and NiO/CN-5:1 are confirmed by energy dispersive spectrometer from scanning electron microscopy (Figure S1a–c of the Supporting Information), which is close to the ratio set in synthetic process.

The typical morphology of fabricated products is characterized. The transmission electron microscopy (TEM) image of CN is presented in **Figure 2**a, clearly showing the smooth sheet structure with curly edge. For the fabricated NiO product, the TEM image in Figure 2b exhibits that the product is particle-like morphology with average size as about 100 nm. The enlarged TEM image in Figure 2c shows that each particle is composed of aggregated nanocrystals with size about 5–8 nm. The TEM image of NiO/CN-2:1 is shown in Figure 2d, clearly showing that the NiO nanocrystals are uniformly distributed on surface of CN nanosheets. The enlarged TEM image in Figure 2e illustrates that the size of NiO nanocrystals is from 10 to 20 nm, which is slightly increased in comparison with Figure 2c. A high-resolution transmission electron microscopy (HRTEM) image of NiO/CN (Figure 2f) displays a nanoparticle with lattice fringe distance of ≈0.21 nm, which corresponds to the (200) face of NiO. Such a result strongly confirms that the NiO nanocrystal anchors on the surface of g-C_3N_4. The high-angle annular dark-field scanning transmission electron microscopy (HAADF-STEM) image in Figure 2g clearly exhibits that the NiO nanoparticles are dispersed throughout the whole surface of CN nanosheet. And the magnified area of HAADF-STEM in Figure 2h reveals that the dispersed NiO nanocrystals have a size distribution of 10–20 nm. The energy dispersive X-ray (EDX) elemental mapping images are obtained from Figure 2h, demonstrating that the C and N elements are only distributed on nanosheets, whereas the Ni and O elements only exist on surface anchored nanocrystals (Figure 2i). On the basis

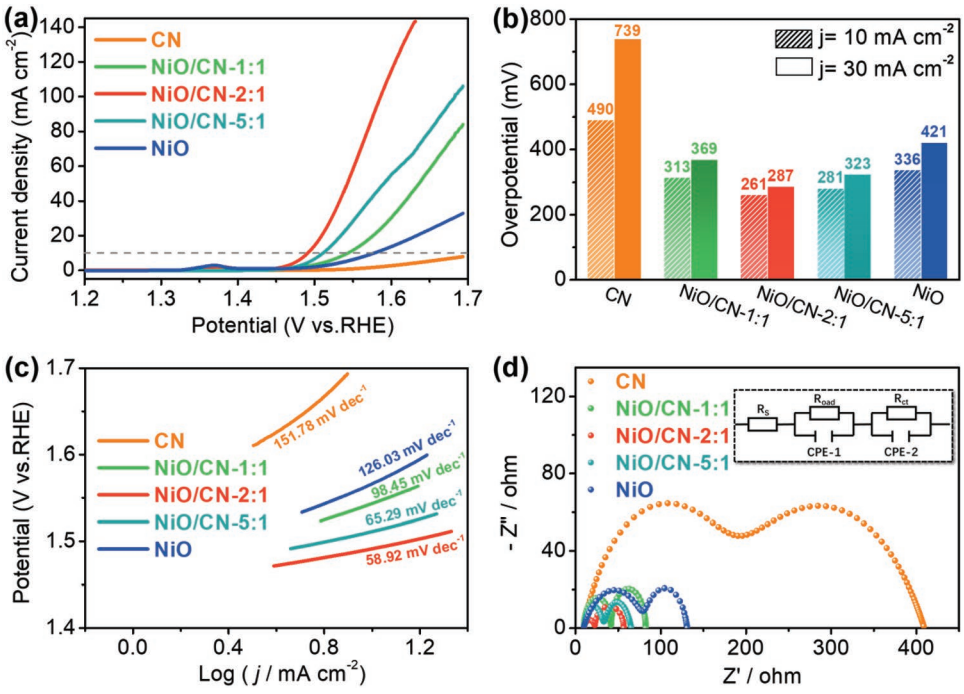

Figure 3. OER performance of the CN, NiO/CN-1:1, NiO/CN-2:1, NiO/CN-5:1, and NiO catalysts in 1 M KOH: a) polarization curves at a scan rate of 10 mV s^{-1} and b) the corresponding overpotential at 10 and 30 mA cm^{-2}; c) Tafel plots derived from corresponding polarization curves; d) Nyquist plots at a constant potential of 1.55 V versus RHE (the inset is the model of equivalent circuit).

of the above results, it can be certainly concluded that NiO nanocrystals are uniformly grown on surface of CN to generate a NiO/CN composite.

In the following study, electrocatalytic oxygen evolution reaction behavior of products synthesized with different ratio of CN and NiO was evaluated by using 1 M KOH solution as electrolyte. The linear sweep voltammetry (LSV) curves of these catalysts were recorded with iR-corrected at a scan rate of 10 mV s^{-1}. As displayed in **Figure 3**a, the LSV of CN shows a huge OER potential, indicating that there is almost no activity for this material. After compositing with NiO, obvious OER polarization curves are produced and the OER potential decreases with increasing ratio of NiO and CN from 1:1 to 2:1. Then, the OER potential increases when the ratio of NiO and CN is further improved from 5:1 to 1:0. Therefore, the ratio of NiO and CN set as 2:1 (NiO/CN-2:1) is a relatively optimal condition among these products. Figure 3b displays the overpotentials of these electrocatalysts to achieve 10 mA cm^{-2}. The NiO and CN require overpotential of 336 and 490 mV to reach current density of 10 mA cm^{-2}, respectively. Otherwise, the NiO/CN-1:1, NiO/CN-2:1, and NiO/CN-5:1 exhibit overpotentials of 313, 261, and 281 mV, respectively. The OER kinetics of these materials were analyzed by Tafel plots as exhibited in Figure 3c. As same to the tendency of LSV curves, the slope for NiO/CN-2:1 is 58.92 mV dec^{-1}, which is distinctly smaller than single phased NiO (110.13 mV dec^{-1}) and CN (151.78 mV dec^{-1}). The OER kinetics over NiO/CN-2:1 also shows superior performance to NiO/CN-1:1 (98.45 mV dec^{-1}) and NiO/CN-5:1 (65.29 mV dec^{-1}). The promoted OER kinetic is associated with improved electron transmission over composited NiO and CN.[35] Hence, the best OER performance can be achieved by properly compositing NiO with CN and the optimized condition is appeared in NiO/CN-2:1. It is known that the resistance of catalysts is important for the electron transmission in OER. To reveal the variety of resistance between these products, the electrochemical impedance spectra (EIS) of these electrodes is recorded and compared. It is shown that there are two clear semicircles are presented in Nyquist plots. The semicircle in high frequency is corresponding to a charge transfer resistance (R_{ct}) between the surface of the electrocatalyst and electrolyte.[36] The semicircle in low-frequency is associated with the adsorptive or formative resistance (R_{oad}) of surface intermediates (e. g., O_{ad}) in the faradaic process, which reflects the mass transfer ability. Both R_{ct} and R_{oad} are directly related to OER kinetics. In addition, there is solution resistance (R_s), which relates to the resistance of electrolyte.[36] For better comparison of these materials, a model of equivalent circuit (inset of Figure 3d) was built to fit the spectra of EIS. The value of R_s, R_{ct}, and R_{oad} were obtained by fitting the EIS curves in Table S1 of the Supporting Information. The calculated values of R_s for these electrodes are almost unchanged (≈9.8 ± 0.2 Ω), indicating all products are measured under a same electrochemical condition. The R_{ct} for NiO, g-C_3N_4, NiO/CN-1:1, NiO/CN-2:1, and NiO/CN-5:1 are 49.2, 230.6, 32.6, 13.4, and 22.9 Ω, respectively. The composited NiO/CN shows reduced resistance than single phased NiO and CN and the optimized product is located at NiO/CN-2:1. The trend of R_{oad} is same as R_{ct}, where NiO, g-C_3N_4, NiO/CN-1:1, NiO/CN-2:1, and NiO/CN-5:1 exhibits R_{oad} as 72.5, 169.2, 40.1, 28.6, and 32.6 Ω, respectively. These results strongly suggest that the resistance for charge transmission and intermediates adsorption resistance can be distinctly reduced through compositing NiO and g-C_3N_4.

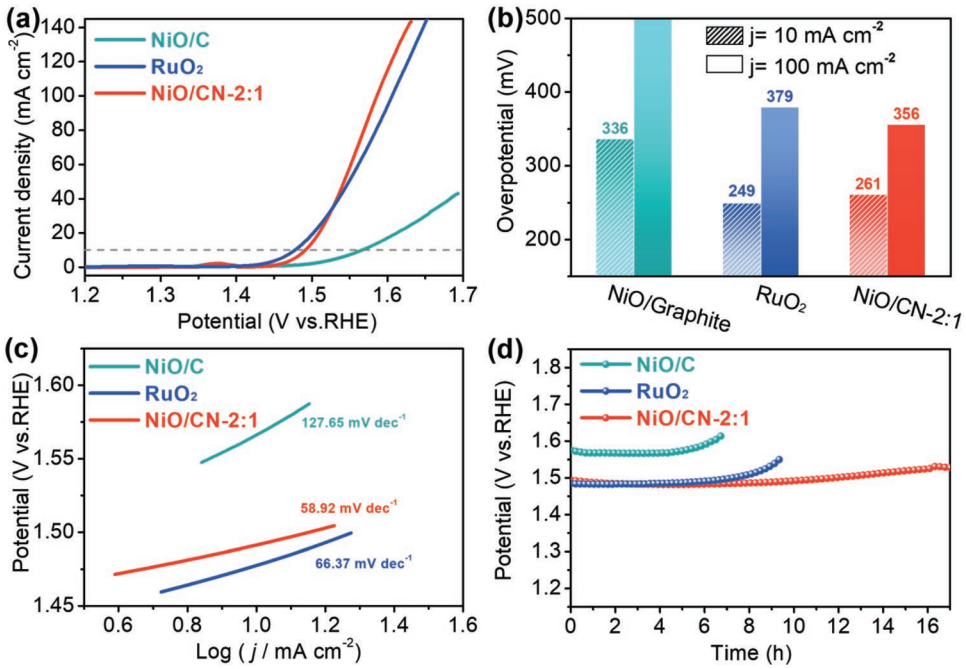

Figure 4. OER performance of the NiO/C, NiO/CN, and commercial RuO_2 catalysts in 1 M KOH: a) Polarization curves at a scan rate of 10 mV s^{-1} and b) the calculated overpotentials at 10 and 100 mA cm^{-2}; c) Tafel plots derived from corresponding polarization curves; d) chronopotentiometry curves of NiO/C, NiO/CN, and commercial RuO_2 under a constant current density of 10 mA cm^{-2}.

For comparison purpose, the NiO composited with conductive graphite (NiO/C, the ratio of NiO and C is 2:1) are synthesized at similar condition. The OER behavior for NiO/C and noble metal–based compound such as commercial RuO_2 (Alfa Aesar Corp.) are evaluated at same condition as NiO/CN-2:1. **Figure 4**a shows the LSV curves of NiO/C, RuO_2, and NiO/CN-2:1. It is observed that NiO/CN-2:1 shows much decreased potential than the NiO/C. The NiO/CN-2:1 shows slightly larger OER potential than RuO_2 when current density is lower than 40 mA cm^{-2}. With the increase of applied potential, the anodic current density of NiO/CN-2:1 rises fast and the NiO/CN-2:1 shows obvious lower potentials than RuO_2 when the current density is above 40 mA cm^{-2}. As Figure 4b illustrated, the overpotentials of NiO/CN-2:1 (261 mV) is much lower than NiO/C (336 mV) and higher than commercial RuO_2 (249 mV) under 10 mA cm^{-2}. However, when anodic current density reached 100 mA cm^{-2}, the overpotential of the NiO/CN-2:1 (356 mV) is obviously superior to RuO_2 (379 mV). The Tafel slope (Figure 4c) of 58.92 mV dec^{-1} for NiO/CN is smaller than 66.37 mV dec^{-1} of RuO_2 and 127.65 mV dec^{-1} of NiO/C. Moreover, the excellent OER performance for optimized NiO/CN is also superior to mostly previously reported NiO-based catalysts that was tested at similar environment as shown in **Table 1**, demonstrating that the construction of NiO and CN composite is a promising strategy to reduce the overpotential and promote the reaction kinetics. The stability in OER of these materials is compared in chronopotentiometry (CP) plots as illustrated in Figure 4d. The potential of NiO/CN-2:1 can be kept at about 1.49 V to reach 10 mA cm^{-2} for 16 h, which is more stable than 8 h of commercial RuO_2 and 6 h of NiO/C. The NiO/CN-2:1, thus, possess more favorable stability than that of NiO/C and

Table 1. Comparisons of OER performance over Ni-based catalysts in alkaline medium.

Catalyst	WE[a)]	Electrolyte [M KOH]	J[b)]	η[c)]	TS[d)]	Ref.
NiO/Co_3O_4@NC	GC	1	10	260	73	[52]
Ni-MOF	GC	1	10	280	64	[53]
$Ni_{2-x}Fe_xO$	GC	0.5	10	325	53	[54]
Ni_2P	GC	1	10	320	105	[16]
Ni-Fe-NCs	GC	1	10	271	48	[54]
NiO-NPs	GC	1	10	481	238	[55]
NiO/MnO_2	GC	0.1	10	345	42	[56]
N-NiO	GC	0.1	10	400	56	[57]
NiO/Ni-Fe LDH	GC	1	10	270	30	[58]
NiO NRs	GC	6	10	390	/	[59]
Pt/NiO	GC	1	10	358	33	[60]
NiO_x/P-CNTs	GC	0.1	10	350	40	[61]
$NiCo_2P_x$/ CNTs	GC	1	10	284	50.3	[62]
Ni_3Se_2	GC	1	10	310	97.1	[63]
Ni_3N	GC	1	10	290	45	[39]
Ni_3FeN/r-GO	GC	1	10	270	94	[41]
Ni-N-O	GC	1	10	300	74	[7]
Ni_3B	GC	1	10	302	52	[64]
NiO/CN	GC	1	10	261	58.9	This work

[a)]WE is working electrode (GC, Glass carbon); [b)]J is current density (mA cm^{-2}); [c)]η is overpotential (mV); [d)]TS is Tafel slope (mV dec^{-1}).

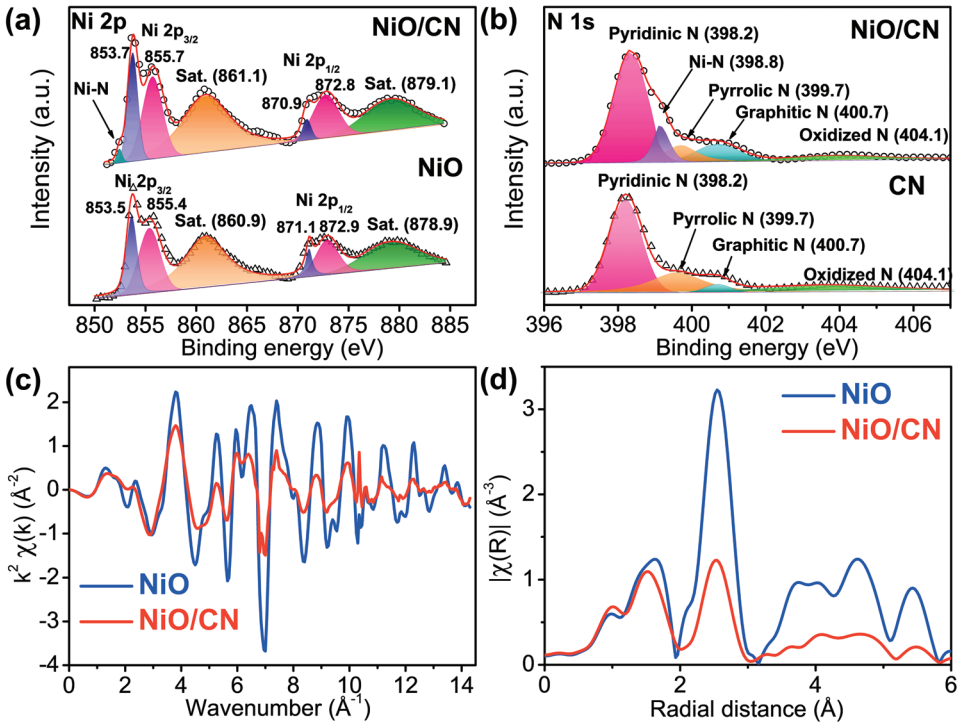

Figure 5. a) Ni 2p and b) N 1s XPS spectra of the NiO/CN-2:1; synchrotron radiation XAFS spectra of NiO/CN and NiO for c) Ni K-edge extended XAFS oscillation function $k^2\chi(k)$ and d) the corresponding Fourier transform curves.

commercial RuO_2. The improved stability over NiO/CN-2:1 is due to the synergetic effects over NiO and CN in that the good mechanical strength of g-C_3N_4 can act as substrate to suppress NiO nanocrystallines aggregating and falling off from the glassy carbon electrode.[31,32] The NiO/CN-2:1 after OER test is also characterized by XRD as displayed in Figure S2 of the Supporting Information. Besides the NiO, the NiOOH is appeared because of the oxidation in long-term OER tests. In our OER measurements, the Pt plat is used as counter electrode. To exclude the Pt deposition effect on working electrode, LSV curves and CP plots are compared by using Pt plat and carbon rod as counter electrodes. As shown in Figure S3 of the Supporting Information, the LSV curves and CP plots are almost overlapped over NiO/CN-2:1 material, suggesting that the OER performance of the fabricated materials is reliable.

Besides for alkaline media, the OER behavior of these catalysts is also evaluated in neutral aqueous electrolyte (0.05 M phosphatic buffer solution (PBS), pH = 6.9). The LSV curves in Figure S4a in the Supporting Information illustrate that the NiO/CN-2:1 shows higher current density than NiO in all applied potential. The current density over NiO/CN-2:1 increase faster than RuO_2 with the increase in the applied potential. As Figure S4b in the Supporting Information exhibited, the NiO/CN-2:1 requires overpotential of 458 mV to reach current density of 1 mA cm^{-2}, which is much lower than NiO (507 mV) and higher than RuO_2 (306 mV). Moreover, to reach a high current density of 30 mA cm^{-2}, NiO/CN-2:1 needs overpotential of 666 mV, which is obviously lower than the RuO_2 (706 mV). Meanwhile, the Tafel slope for NiO/CN-2:1 in Figure S4c in the Supporting Information was 131.6 mV dec^{-1}, which is obviously smaller than NiO (242.72 mV dec^{-1}) and commercial RuO_2 (241.45 mV dec^{-1}), suggesting a much promoted OER kinetics over NiO/CN-2:1 than the NiO and RuO_2. Finally, the durability of NiO/CN-2:1 in 0.05 M PBS electrolyte at 10 mA cm^{-2} is confirmed by CP. As illustrated in Figure S4d in the Supporting Information, the working potential over NiO/CN-2:1 can keep stable before 6 h, which is more stable than 3 h of NiO and 4 h of commercial RuO_2.

To make clear the possible mechanism for the enhancement of the OER performance over NiO/CN-2:1, the surface chemical states of NiO/CN-2:1 were studied by X-ray photoelectron spectroscopy (XPS) first. The NiO, CN, and NiO/CN-2:1 were selected as representative samples for XPS analysis. The C 1s at 284.6 eV from adventitious carbon was used to calibrate the XPS spectra. As shown from the Ni 2p spectrum of NiO (**Figure 5**a), a peak at 853.7 eV is assigned to Ni $2p_{3/2}$ and another peak at 871.1 eV is assigned to Ni $2p_{1/2}$, which suggests the existence of Ni^{3+}.[37] Besides for that, split peaks at 855.7 and 872.8 eV are assigned to Ni $2p_{3/2}$ and Ni $2p_{1/2}$, respectively, referring to the state of Ni^{2+}.[38] For the Ni 2p XPS spectrum of NiO/CN-2:1, a slightly shift (0.1–0.3 eV) of Ni $2p_{3/2}$ and Ni $2p_{1/2}$ to higher bonding energy is observed, indicating that the environment of surface Ni atom in NiO is changed after coupling with CN. It should be noted that there is a weak peak of 852.4 eV in NiO/CN-2:1, which can be identified as Ni–N bond.[39–41] Such results indicate that NiO and CN are not simply physical mixture, but formed chemical bonds at interface. To further clarify the existence of such a bond, the N 1s XPS spectrum was also checked. The XPS spectrum for bare CN (Figure 5b) are divided into four peaks at 398.2, 399.7, 400.7, and 404.1 eV, corresponding to pyridinic N, pyrrolic N, graphitic N, and oxidized N, respectively.[42–44] These four peaks are also existed in XPS

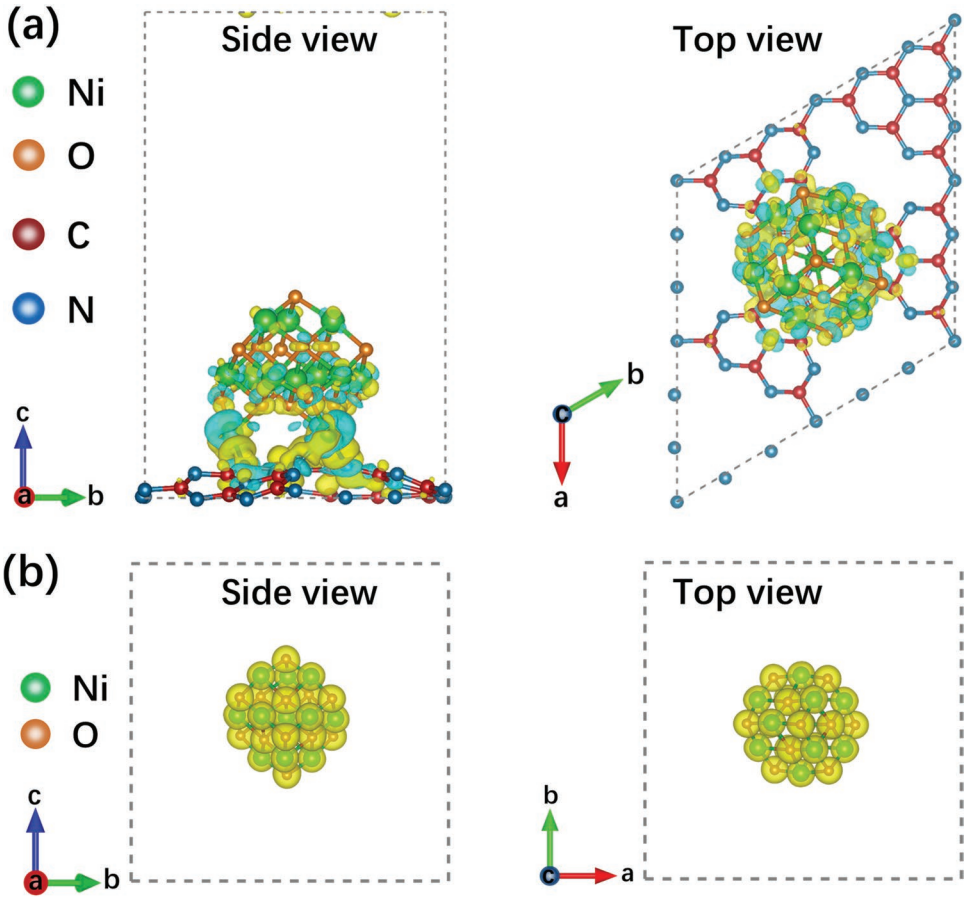

Figure 6. Interfacial electron transfer in a) NiO/CN and b) NiO (yellow and cyan isosurfaces represent electron accumulation and electron depletion, respectively, the isosurface value is 0.001 e Å^{-3}).

spectra of NiO/CN-2:1. Besides for that, there is an obvious split peak at about 398.5 eV, which can readily be assigned to Ni–N bond.[7,39,45] To further study the chemical bonding information, the extended X-ray absorption fine structure (EXAFS) spectra were performed and displayed in Figure 5c,d. It can be seen from the $K^2\chi(k)$ plots in that the amplitude of $K^2\chi(k)$ oscillations in NiO/CN-2:1 is much smaller than that of NiO, indicating that the crystal lattice of NiO/CN-2:1 is more distorted than that of NiO.[46] From the $|\chi(R)|$ plots, a shoulder locates at about 2.1 Å in NiO curve can be observed, which corresponds to the typical Ni–O bonds in the NiO.[47] However, the shoulder almost disappears in the NiO/CN-2:1 curve, which can be ascribed to the destructive interference of oscillations from Ni–N and Ni–O bonds when Ni–N bonds exist concurrently.[48] On the basis of above analysis, the Ni–N is produced in composites of NiO and CN. It is widely reported that the Ni–N bond is metallic and nickel nitride such as Ni_3N, Ni–N_x, and Ni–N–C are high conductive materials.[39,40,45] The conductive interface is, thus produced between NiO with CN through compositing, which induces a much reduced R_{ct} in OER as depicted EIS analysis of Figure 3d.

To examine influences of formed Ni–N bond on inherent electronic distribution of the material, an atomic model is built in Figure S5 of the Supporting Information. For the atomic model of CN, the g-C_3N_4 with a 2 × 2 × 1 unit cell is cut into one layer atomic slab (Figure S5a, Supporting Information). The atomic model of NiO nanocrystal is constructed by a $Ni_{13}O_{14}$ cluster (Figure S5b, Supporting Information). To simulate NiO nanocrystals anchored on g-C_3N_4, the NiO nanocluster is linked with single layer g-C_3N_4 (Figure S5c, Supporting Information) by Ni–N bonds. The calculation based on density functional theory shows that the redistribution of the charge density is occurred near the NiO/CN interface as illustrated in **Figure 6**a,b. There is vast electrons accumulation to the Ni atoms near the Ni–N bonds at interface. Such an accumulation is wreaked at the Ni atoms that are slightly far away from Ni–N bonds. For comparison, the charge distribution over NiO cluster is also calculated (Figure 6c,d), displaying that there is no obvious accumulation near Ni atoms over pure NiO. On the basis of above discussion, the interfacial Ni–N bonds induces the charge accumulation to the Ni atoms, which is beneficial to adsorb and activate the reaction intermediates of OER.[49]

Inspired by such a result, the adsorption ability of OER intermediates over NiO/CN and NiO atomic models was studied. The Gibbs free energy for intermediates adsorptions such as *OH, *O, and *OOH were calculated by the density functional theory plus U (DFT+U). The OER is considered as a four-step electron transfer process, where surface Ni site is realized as adsorption site to bind oxygen intermediates. The optimized calculation models are built in Figure S6 of the Supporting

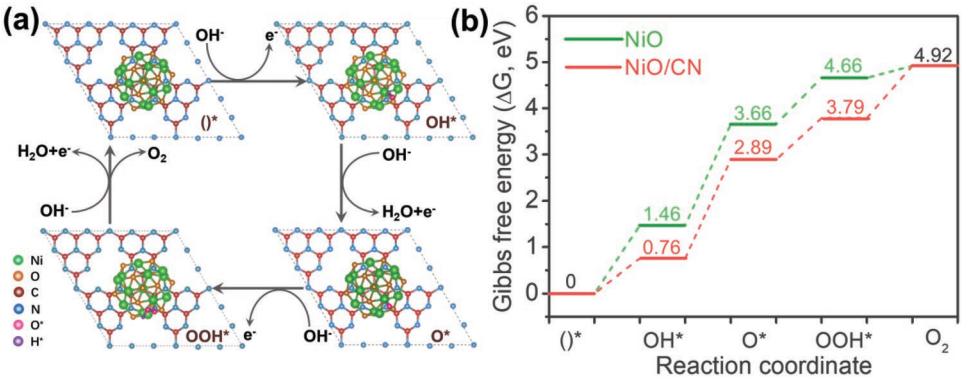

Figure 7. a) The atomic pathway of OER on surface of NiO/CN; b) Gibbs free energy of absorbed H_2O, OH*, O*, OOH*, and O_2 for NiO and NiO/CN.

Information. **Figure 7**a displays the possible OER pathway on the surfaces of NiO/CN in alkaline media. The OER is supposed to involve four reaction steps of ()*→OH*, OH*→O*, O*→OOH*, and OOH*→()*+O_2 (()* stands for bare surfaces). The calculated Gibbs free energy level of each step for NiO and NiO/CN are shown in Figure 7b. The adsorption Gibbs free energy is 0.76, 2.89, 3.79, and 4. 92 eV over NiO/CN to produce OH*, O*, OOH*, and O_2, respectively. The adsorption Gibbs free energy of intermediates (H*, O*, OOH*) over NiO/CN is distinctly lower than NiO, which require 1.46, 3.66, and 4.66 eV to adsorb H*, O*, OOH*, respectively. Therefore, the NiO/CN interface with Ni–N bonds can effectively minimize the adsorption energy barriers of OER intermediates, which results minimized R_{oad} shown in EIS analysis (Figure 3d) and benefits the intermediates adsorption in OER.

Some other factors also influenced the OER efficiency. For instance, the CN could act as substrate for dispersing NiO nanocrystals and prevent nanoparticles aggregating, which provided more active sites and promote the OER performance.[31,50] The electrochemical active surface area (ESCA) was thus analyzed as shown in Figure S7a of the Supporting Information. The calculated double layer capacitance (C_{dl}) value over NiO/CN-2:1 are 43.73 mF cm^{-2}, which is certainly higher than 14.32 mF cm^{-2} of NiO and 3.95 mF cm^{-2} for g-C_3N_4.[24,41] When the current density is normalized with ESCA (Figure S7b of the Supporting Information), the NiO/CN-2:1 still exhibits much lower OER overpotential (316 mV at 0.05 mA cm^{-2}) than NiO (392 mV at 0.05 mAcm^{-2}) and g-C_3N_4 (410 mV at 0.05 mAcm^{-2}), confirming that the intrinsic characteristic from NiO/CN-2:1 material itself, e.g., the high conductivity and strong adsorption intermediates, contribute importantly to the improvement of OER performance over composited NiO/CN.

To further experimentally confirm that the improved OER performance over NiO/CN was come from the existence of interfacial Ni–N bond, a controlled CN supported NiO is fabricated (NiO/CN-Control, see Experimental Section). In such a synthetic method, the dispersed NiO nanocrystals on CN can be obtained (see XRD pattern and TEM image in Figure S8 of the Supporting Information), but it is difficult to get obvious Ni–N bonds as analysed by XPS (Figure S9, Supporting Information). The OER performance over NiO/CN-Control shows much higher overpotential (328 mV at 10 mA cm^{-2}) and larger Tafel slope (105.78 mV dec^{-1}) than NiO/CN-2:1 (Figure S10, Supporting Information). Such a comparison strongly suggests that the produced Ni–N bonds in NiO/CN are main factor resulting the improvement of OER performance.

Such an interfacial high active bond is not only existed between NiO and CN, but also may be existed between CN and other transition metal oxides. Some transition metal oxides (e.g., Co_3O_4, CuO, Fe_2O_3) can also produce improved OER performance when compositing with CN. **Figure 8**a,b displays the OER polarization curves and Tafel slopes of Co_3O_4/CN, CuO/CN, and Fe_2O_3/CN, which were synthesized at same condition as NiO/CN-2:1. In comparison with corresponding pure

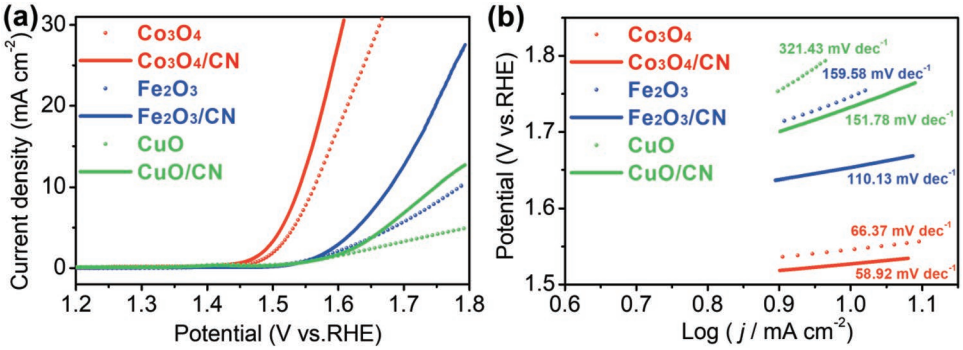

Figure 8. Evaluation of electrocatalytic OER performance of Co_3O_4, Co_3O_4/CN, Fe_2O_3, Fe_2O_3/CN, CuO, and CuO/CN in 1 M KOH: a) iR-corrected linear sweep voltammetry curves and b) corresponding Tafel plots.

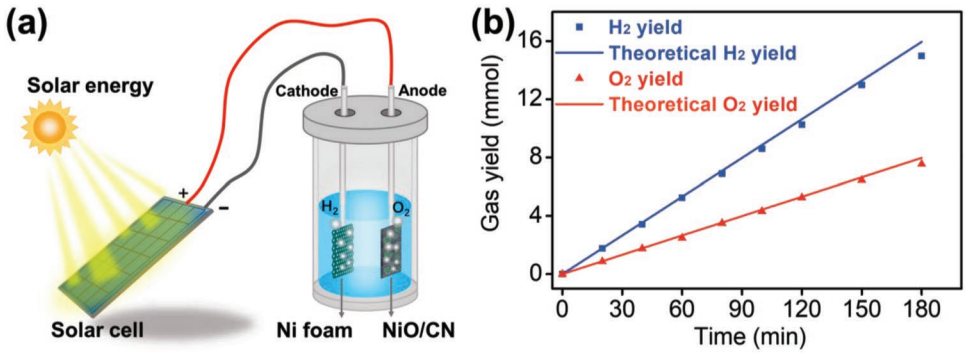

Figure 9. a) The schematic of the solar-to-hydrogen energy conversion by using a solar cell to achieve full water splitting by two-electrode system; b) H_2 and O_2 yields for the cathode and anode in 1 M KOH solution (the blue and red lines represent the gas evolution at 100% Faradaic efficiency; the blue dots and red dots represent the H_2 and O_2 measured by gas chromatography).

metal oxides, all composited material exhibit much lower overpotentials and smaller value Tafel slopes. Meanwhile, these composite materials show distinctly reduced electrochemical resistance as pure transition metal oxides as exhibited from the EIS analysis in Figure S11 of the Supporting Information.

The electrochemical conversion of water into hydrogen through solar are promising for the development of sustainable energy.[1,28,51] To demonstrate the practical application of NiO/CN, an overall water splitting system constructed by connecting two electrodes to a crystalline silicon solar cell (**Figure 9**a, detailed energy conversion device is presented in Figure S12 of the Supporting Information). The Ni foam supported NiO/CN-2:1 and bare Ni foam are used as electrodes for OER and HER, respectively. A Xe lamp with wavelength from 400 to 800 nm is used as light source (Figure S13, Supporting Information). The voltage provided by solar cell on the two-electrode system was kept at 2.45 V by adjusting the intensity of Xe lamp. The rates of evolved H_2 and O_2 from the cathode (Ni foam) and anode (Ni foam supported NiO/CN-2:1) are 5.3 and 2.6 mmol h^{-1}, respectively (Figure 9b). Apparently, the yield of H_2 is nearly twice as much as that of O_2. The theoretical yield of H_2 and O_2 were calculated on the basis of the current of 284.8 mA under 2.45 V, which is determined from the LSV curve (Figure S14, Supporting Information). The Faradaic efficiency for gas evolution is 98.81%. The energy conversion yield of photo-to-H_2 is calculated to be 5.35%, exhibiting a feasible method to convert solar energy into hydrogen energy by using fabricated NiO/CN as catalyst.

3. Conclusions

In summary, composited NiO/CN material with conductive interfaces are constructed by an in situ decomposition method. The as prepared electrocatalysts show highly efficient OER at alkaline and neutral conditions. The optimized NiO/CN-2:1 material requires overpotential of 261 mV to achieve 10 mA cm^{-2} and 580 mV to achieve 1 mA cm^{-2} in 1 M KOH and 0.05 M PBS, respectively. The OER performance over the NiO/CN-2:1 is much superior to that of commonly used NiO/C, commercial RuO_2 catalyst, and mostly reported NiO-based electrodes. XPS and XAFS analysis confirmed that Ni–N bond are generated during the synthetic process, which make the NiO/CN-2:1 possess favourable conductivity. DFT calculations reveal that the NiO/CN with the existence of interfacial Ni–N bond can promote the adsorptions of OER intermediates. These characteristics benefit the reduced charge transfer and mass transfer resistance, which promote the OER performance. It is interesting that such metallic metal–nitrogen bond is not only existed between NiO and CN, but also between CN and other transition metal oxides, including Co_3O_4, CuO, and Fe_2O_3. To demonstrate the application of the as fabricated catalyst, the Ni foam supported NiO/CN and bare Ni foam electrodes are linked with solar cell to form an overall water splitting system. The energy conversion efficiency of solar-to-hydrogen and the Faradaic efficiency are 5.35% and 98.81%, respectively. The composited transition metal oxides and CN reported here show promising prospect as alternatives to noble metal–based catalysts for efficient water splitting. Moreover, this study gives a promising strategy to construct high active interface between poor conductive components, which may also be applied to design catalysts for other electrocatalytic reactions including O_2 reduction, CO_2 reduction, N_2 activation, and so on.

4. Experimental Section

Synthesis of Polymer Carbon Nitride: All chemical reagents were analytic grade without further purifying. Urea (10.0 g) was put into an alumina crucible with a cover and then annealed at 550 °C for 2 h in a muffle furnace. The polymer carbon nitride with a light-yellow colour was obtained after cooling down.

Synthesis of NiO/CN Nanocomposites: In a typical process, 0.05 g g-C_3N_4 was added in 30.0 mL deionized water and then ultrasonic dispersion for 30 min. Subsequently, $Ni(CH_3COO)_2{\cdot}4H_2O$ was added and vigorously stirred for dissolving. The NiO/g-C_3N_4 nanocomposites with a dark-green color were obtained by calcining the solution in air at 350 °C for 2 h. In this work, NiO/carbon nitride composites are written as NiO/CN-m:n, where CN stands for polymer carbon nitride and the m:n is the ratio between Ni and CN set in experiments. The pure NiO was obtained by the same method without the CN addition.

In synthesis of NiO/graphite composites, the synthetic condition was as same to NiO/CN by using graphite instead of g-C_3N_4. The product was marked as NiO/C.

In a control experiment of for synthesizing NiO/g-C_3N_4 composites, the as-synthesized NiO and CN were dispersed in 30 mL deionized water and stirred for 0.5 h. Then the mixture was filtrated and dried

at 60 °C. The obtained powder was calcinated at 350 °C for 2 h. The product was marked as NiO/CN-Control.

The characterizations, calculation details, evaluation of electrocatalysis, and photovoltaic-electrocatalytic water splitting are described in the Supporting Information.

Supporting Information

Supporting Information is available from the Wiley Online Library or from the author.

Acknowledgements

C.L. and B.Y. contributed equally to this work. This work was financially supported by National Natural Science Foundation of China (No. 51874357, 21872174, and 51872333) and Innovative Research Group of Hunan Provincial Natural Science Foundation of China (2019JJ10006).

Conflict of Interest

The authors declare no conflict of interest.

Keywords

conductive interfaces, electrocatalysts, nickel oxide, oxygen evolution reaction, water splitting

Received: May 20, 2019
Revised: July 11, 2019
Published online: August 9, 2019

[1] S. Chu, A. Majumdar, *Nature* **2012**, *488*, 294.
[2] Z. W. Seh, J. Kibsgaard, C. F. Dickens, I. Chorkendorff, J. K. Nørskov, T. F. Jaramillo, *Science* **2017**, *355*, eaad4998.
[3] J. Suntivich, H. A. Gasteiger, N. Yabuuchi, H. Nakanishi, J. B. Goodenough, Y. Shao-Horn, *Nat. Chem.* **2011**, *3*, 546.
[4] J. Tian, Q. Liu, A. M. Asiri, X. Sun, *J. Am. Chem. Soc.* **2014**, *136*, 7587.
[5] M. G. Walter, E. L. Warren, J. R. McKone, S. W. Boettcher, Q. Mi, E. A. Santori, N. S. Lewis, *Chem. Rev.* **2010**, *110*, 6446.
[6] Z. Xiao, Y. Wang, Y. C. Huang, Z. Wei, C. L. Dong, J. Ma, S. Shen, Y. Li, S. Wang, *Energy Environ. Sci.* **2017**, *10*, 2563.
[7] J. Huang, Y. Sun, X. Du, Y. Zhang, C. Wu, C. Yan, Y. Yan, G. Zou, W. Wu, R. Lu, Y. Li, J. Xiong, *Adv. Mater.* **2018**, *30*, 1.
[8] Z. Li, W. Niu, L. Zhou, Y. Yang, *ACS Energy Lett.* **2018**, *3*, 892.
[9] M. Tahir, L. Pan, R. Zhang, Y. C. Wang, G. Shen, I. Aslam, M. A. Qadeer, N. Mahmood, W. Xu, L. Wang, X. Zhang, J. J. Zou, *ACS Energy Lett.* **2017**, *2*, 2177.
[10] L. Ma, S. Chen, H. Li, Z. Ruan, Z. Tang, Z. Liu, Z. Wang, Y. Huang, Z. Pei, J. A. Zapien, C. Zhi, *Energy Environ. Sci.* **2018**, *11*, 2521.
[11] Y. Wang, C. Xie, Z. Zhang, D. Liu, R. Chen, S. Wang, *Adv. Funct. Mater.* **2018**, *28*, 1703363.
[12] X. Jia, Y. Zhao, G. Chen, L. Shang, R. Shi, X. Kang, G. I. N. Waterhouse, L.-Z. Wu, C.-H. Tung, T. Zhang, *Adv. Energy Mater.* **2016**, *6*, 1502585.
[13] Y. Jin, S. Huang, X. Yue, H. Du, P. K. Shen, *ACS Catal.* **2018**, *8*, 2359.
[14] D. Zhou, Z. Cai, X. Lei, W. Tian, Y. Bi, Y. Jia, N. Han, T. Gao, Q. Zhang, Y. Kuang, J. Pan, X. Sun, X. Duan, *Adv. Energy Mater.* **2018**, *8*, 1701905.
[15] X. Y. Yu, Y. Feng, B. Guan, X. W. D. Lou, U. Paik, *Energy Environ. Sci.* **2016**, *9*, 1246.
[16] Q. Wang, Z. Liu, H. Zhao, H. Huang, H. Jiao, Y. Du, *J. Mater. Chem. A* **2018**, *6*, 18720.
[17] T. Wang, L. Liu, Z. Zhu, P. Papakonstantinou, J. Hu, H. Liu, M. Li, *Energy Environ. Sci.* **2013**, *6*, 625.
[18] Y. Guo, T. Park, J. W. Yi, J. Henzie, J. Kim, Z. Wang, B. Jiang, Y. Bando, Y. Sugahara, J. Tang, Y. Yamauchi, *Adv. Mater.* **2019**, *31*, 1807134.
[19] S. J. Pennycook, M. Guan, J. Yang, M.-C. Tsai, Y. Hu, M. Gong, W. Zhou, J. Zhou, B.-J. Hwang, H. Dai, D.-Y. Wang, M.-C. Lin, B. Zhang, *Nat. Commun.* **2014**, *5*, 1.
[20] J. Qiao, Y. Liu, F. Hong, J. Zhang, *Chem. Soc. Rev.* **2014**, *43*, 631.
[21] J. Zhang, J. Wu, H. Guo, W. Chen, J. Yuan, U. Martinez, G. Gupta, A. Mohite, P. M. Ajayan, J. Lou, *Adv. Mater.* **2017**, *29*, 1701955.
[22] Y. Li, C. Liao, K. Tang, N. Zhang, W. Qi, H. Xie, J. He, K. Yin, Y. Gao, C. Wang, *Electrochim. Acta* **2019**, *297*, 40.
[23] X. Ren, J. Zhou, X. Qi, Y. Liu, Z. Huang, Z. Li, Y. Ge, S. C. Dhanabalan, J. S. Ponraj, S. Wang, J. Zhong, H. Zhang, *Adv. Energy Mater.* **2017**, *7*, 1700396.
[24] W. Ma, R. Ma, C. Wang, J. Liang, X. Liu, K. Zhou, T. Sasaki, *ACS Nano* **2015**, *9*, 1977.
[25] H. Tan, J. Tang, J. Henzie, Y. Li, X. Xu, T. Chen, Z. Wang, J. Wang, Y. Ide, Y. Bando, Y. Yamauchi, *ACS Nano* **2018**, *12*, 5674.
[26] H. Tan, Y. Li, J. Kim, T. Takei, Z. Wang, X. Xu, J. Wang, Y. Bando, Y. M. Kang, J. Tang, Y. Yamauchi, *Adv. Sci.* **2018**, *5*.
[27] Y. Guo, J. Tang, J. Henzie, B. Jiang, H. Qian, Z. Wang, H. Tan, Y. Bando, Y. Yamauchi, *Mater. Horiz.* **2017**, *4*, 1171.
[28] W. Niu, Z. Li, K. Marcus, L. Zhou, Y. Li, R. Ye, K. Liang, Y. Yang, *Adv. Energy Mater.* **2018**, *8*, 1.
[29] M. Shalom, S. Gimenez, F. Schipper, I. Herraiz-Cardona, J. Bisquert, M. Antonietti, *Angew. Chem., Int. Ed.* **2014**, *53*, 3654.
[30] M. Volokh, G. Peng, J. Barrio, M. Shalom, *Angew. Chemie Int., Ed.* **2019**, *58*, 6138.
[31] S. Zhao, Z. Tang, S. Guo, M. Han, C. Zhu, Y. Zhou, L. Bai, J. Gao, H. Huang, Y. Li, Y. Liu, Z. Kang, *ACS Catal.* **2018**, *8*, 188.
[32] Z. Zhuang, Y. Li, Z. Li, F. Lv, Z. Lang, K. Zhao, L. Zhou, L. Moskaleva, S. Guo, L. Mai, *Angew. Chem., Int. Ed.* **2018**, *57*, 496.
[33] H. Yu, L. Shang, T. Bian, R. Shi, G. I. N. Waterhouse, Y. Zhao, C. Zhou, L.-Z. Wu, C.-H. Tung, T. Zhang, *Adv. Mater.* **2016**, *28*, 5140.
[34] Y. Li, S. Ouyang, H. Xu, X. Wang, Y. Bi, Y. Zhang, J. Ye, *J. Am. Chem. Soc.* **2016**, *138*, 13289.
[35] W. Gao, Z. Xia, F. Cao, J. C. Ho, Z. Jiang, Y. Qu, *Adv. Funct. Mater.* **2018**, *28*, 1.
[36] N. Zhang, B. Yang, Y. He, Y. He, X. Liu, M. Liu, G. Song, G. Chen, A. Pan, S. Liang, R. Ma, S. Venkatesh, V. A. L. Roy, *Small* **2018**, *5*, 1.
[37] H. Chen, L. Hu, M. Chen, Y. Yan, L. Wu, *Adv. Funct. Mater.* **2014**, *24*, 934.
[38] X. F. Lu, D. J. Wu, R. Z. Li, Q. Li, S. H. Ye, Y. X. Tong, G. R. Li, *J. Mater. Chem. A* **2014**, *2*, 4706.
[39] K. Xu, P. Chen, X. Li, Y. Tong, H. Ding, X. Wu, W. Chu, Z. Peng, C. Wu, Y. Xie, *J. Am. Chem. Soc.* **2015**, *137*, 4119.
[40] J. Yin, Q. Fan, Y. Li, F. Cheng, P. Zhou, P. Xi, S. Sun, *J. Am. Chem. Soc.* **2016**, *138*, 14546.
[41] Y. Gu, S. Chen, J. Ren, Y. A. Jia, C. Chen, S. Komarneni, D. Yang, X. Yao, *ACS Nano* **2018**, *12*, 245.
[42] X. Li, W. Bi, M. Chen, Y. Sun, H. Ju, W. Yan, J. Zhu, X. Wu, W. Chu, C. Wu, Y. Xie, *J. Am. Chem. Soc.* **2017**, *139*, 14889.

[43] L. Ye, G. Chai, Z. Wen, *Adv. Funct. Mater.* **2017**, *27*.
[44] H. Tan, Y. Li, X. Jiang, J. Tang, Z. Wang, H. Qian, P. Mei, V. Malgras, Y. Bando, Y. Yamauchi, *Nano Energy* **2017**, *36*, 286.
[45] C. Lei, Y. Wang, Y. Hou, P. Liu, J. Yang, T. Zhang, X. Zhuang, M. Chen, B. Yang, L. Lei, C. Yuan, M. Qiu, X. Feng, *Energy Environ. Sci.* **2019**, *12*, 149.
[46] K. I. Pandya, R. W. Hoffman, J. Mcbreen, W. E. O'Grady, *Electrochim. Acta* **1983**, *28*, 439.
[47] Y. Hu, I. T. Bae, Y. Mo, D. A. Scherson, M. R. Antonio, *Can. J. Chem.* **1997**, *75*, 1721.
[48] Y. Iwasawa, *X-Ray Absorption Fine Structure for Catalysts and Surfaces*, vol. *2*, World Scientific, Singapore **1996**.
[49] Y. Liu, C. Xiao, P. Huang, M. Cheng, Y. Xie, *Chem* **2018**, *4*, 1263.
[50] J. ying Tang, R. tang Guo, W. guo Zhou, C. ying Huang, W. guo Pan, *Appl. Catal., B* **2018**, *237*, 802.
[51] W. A. Goddard III, J. Sun, R. He, Z. Zhu, Y. Huang, Z. Ren, F. Yu, S. Chen, R. J. Nielsen, H. Zhou, J. Bao, *Nat. Commun.* **2016**, *7*, 1.
[52] G. Shen, L. Wang, N. Mahmood, L. Pan, W. Xu, M. A. Qadeer, I. Aslam, X. Zhang, M. Tahir, Y.-C. Wang, R. Zhang, J.-J. Zou, *ACS Energy Lett.* **2017**, *2*, 1327.
[53] J. Chen, Y. Lin, S. X. Dou, W. Huang, W. Sun, Q. Zhou, J. Zhu, Y. Chen, G. Zhao, K. Rui, *Adv. Funct. Mater.* **2018**, *28*, 1801554.
[54] A. C. Pebley, E. Decolvenaere, T. M. Pollock, M. J. Gordon, *Nanoscale* **2017**, *9*, 15070.
[55] A. Kumar, S. Bhattacharyya, *ACS Appl. Mater. Interfaces* **2017**, *9*, 41906.
[56] J. He, M. Wang, W. Wang, R. Miao, W. Zhong, S. Y. Chen, S. Poges, T. Jafari, W. Song, J. Liu, S. L. Suib, *ACS Appl. Mater. Interfaces* **2017**, *9*, 42676.
[57] T. Zhang, P. Xi, X. Jiang, J. Li, D. Xue, T. Wang, B. Xia, D. Gao, *J. Mater. Chem. A* **2019**, 4729.
[58] J.-Y. Liu, Z.-W. Gao, H. Liu, J. Mao, L. Li, X.-M. Chen, W.-C. Wang, X.-W. Du, T. Ma, X.-L. Zheng, *Adv. Mater.* **2019**, *1804769*, 1804769.
[59] T. Zhang, M. Y. Wu, D. Y. Yan, J. Mao, H. Liu, W. Bin Hu, X. W. Du, T. Ling, S. Z. Qiao, *Nano Energy* **2018**, *43*, 103.
[60] C. Lin, Y. Zhao, H. Zhang, S. Xie, Y. F. Li, X. Li, Z. Jiang, Z. P. Liu, *Chem. Sci.* **2018**, *9*, 6803.
[61] L. Han, S. Dong, E. Wang, *Adv. Mater.* **2016**, *28*, 9266.
[62] C. Huang, T. Ouyang, Y. Zou, N. Li, Z. Q. Liu, *J. Mater. Chem. A* **2018**, *6*, 7420.
[63] A. T. Swesi, J. Masud, M. Nath, *Energy Environ. Sci.* **2016**, *9*, 1771.
[64] W. J. Jiang, S. Niu, T. Tang, Q. H. Zhang, X. Z. Liu, Y. Zhang, Y. Y. Chen, J. H. Li, L. Gu, L. J. Wan, J. S. Hu, *Angew. Chem., Int. Ed.* **2017**, *56*, 6572.